

Lattice-Boltzmann Very Large Eddy Simulation of a Multi-Orifice Acoustic Liner with Turbulent Grazing Flow

Avallone, Francesco; Manjunath, Pranav; Ragni, Daniele; Casalino, Damiano

DOI

[10.2514/6.2019-2542](https://doi.org/10.2514/6.2019-2542)

Publication date

2019

Document Version

Final published version

Published in

25th AIAA/CEAS Aeroacoustics Conference

Citation (APA)

Avallone, F., Manjunath, P., Ragni, D., & Casalino, D. (2019). Lattice-Boltzmann Very Large Eddy Simulation of a Multi-Orifice Acoustic Liner with Turbulent Grazing Flow. In *25th AIAA/CEAS Aeroacoustics Conference: 20-23 May 2019 Delft, The Netherlands* Article AIAA 2019-2542 <https://doi.org/10.2514/6.2019-2542>

Important note

To cite this publication, please use the final published version (if applicable).
Please check the document version above.

Copyright

Other than for strictly personal use, it is not permitted to download, forward or distribute the text or part of it, without the consent of the author(s) and/or copyright holder(s), unless the work is under an open content license such as Creative Commons.

Takedown policy

Please contact us and provide details if you believe this document breaches copyrights.
We will remove access to the work immediately and investigate your claim.



Lattice-Boltzmann Very Large Eddy Simulation of a Multi-Orifice Acoustic Liner with Turbulent Grazing Flow

Francesco Avallone ^{*}, Pranav Manjunath [†], Daniele Ragni [‡] and Damiano Casalino [§]
Delft University of Technology, Kluyverweg 1, 2629HS, Delft, The Netherlands

A lattice-Boltzmann Very Large Eddy simulation of a multi-orifice acoustic liner, grazed by a turbulent flow at Mach number equal to 0.3 and a planar acoustic wave with amplitude equal to 130 dB and frequency equal to 1800 Hz, is carried out. The geometry of the liner replicates the experiments carried out in the Grazing Flow Impedance Tube (GFIT) facility at NASA Langley. It is found that the impedance, obtained from numerical simulations using the Dean's method, is a function of the orifice location. This is attributed to two phenomena: the interaction between the wake behind the upstream orifices and the downstream ones; and the interaction between the flow fields in the cavity induced by the ejected vortices. Results show that, for the investigated configuration, two vortical structures are generated in the orifice: one, formed along the downstream inner wall of the orifice, weakly penetrates into the cavity; the second, formed at the bottom downstream corner of the orifice, is ejected into the cavity up to three orifice diameters. The direction along which the latter is ejected varies with the orifice location. The ejected vortices are characterized by an annular vortex and a trailing vortex similarly to what found for synthetic jets. In the cavity, large scale vortical structures are found. On the face sheet, it is found that the turbulent wakes behind the upstream orifices increases the vertical velocity component within the orifices. These findings suggest that local measurement techniques, such as the Dean's method, might be affected by the sampling location in realistic configurations.

Nomenclature

c	=	sound speed [m/s ²]
d	=	orifice diameter [m]
d_c	=	depth of the cavity [m]
f	=	frequency [Hz]
i	=	imaginary unit
l_c	=	maximum width of the cavity [m]
M	=	Mach number [-]
k_a	=	acoustic wavenumber [-]
p	=	pressure [Pa]
Re	=	Reynolds number [x]
t	=	time [s]
x, y, z	=	streamwise, wall-normal and spanwise direction [m]
x_t	=	streamwise location downstream of the trip [m]
u, v, z	=	streamwise, wall-normal and spanwise velocity components [m/s]
u', v', z'	=	streamwise, wall-normal and spanwise velocity component fluctuations [m/s]
$Z = \theta + i\chi$	=	normalized acoustic impedance, normalized by $\rho_\infty c_\infty$
Greek symbols		
χ	=	normalized acoustic reactance [-]
δ	=	boundary layer thickness [m]
δ^*	=	displacement thickness [m]

^{*} Assistant Professor, Department of Aerodynamic, Wind Energy and Propulsion, f.avallone@tudelft.nl, AIAA member

[†] PhD candidate, Department of Aerodynamic, Wind Energy and Propulsion, p.manjunath@tudelft.nl, AIAA member

[‡] Assistant Professor, Department of Aerodynamic, Wind Energy and Propulsion, d.ragni@tudelft.nl, AIAA member

[§] Full Professor, Department of Aerodynamic, Wind Energy and Propulsion, d.casalino@tudelft.nl, AIAA member

λ_2	=	criterion for vortex identification [s ⁻²]
ϕ	=	phase angle [rad]
ω	=	angular frequency [rad]
ρ	=	density [kg/m ³]
σ	=	porosity [-]
τ	=	face sheet thickness [m]
θ	=	normalized acoustic resistance [-]
Subscript		
a	=	acoustic
b	=	back plate
s	=	face sheet
inc	=	incident
r	=	reflected
t	=	trip
∞	=	free stream

I. Introduction

ACOUSTIC liners are passive control devices used to damp noise caused by fans, compressors or turbines [1]. They reduce noise by dissipating the sound wave energy. The simplest acoustic liner is the single-degree-of-freedom one, where a face sheet with orifices is placed over a honeycomb backing. For this type of liners, the local response depends only on the local acoustic pressure, i.e. they are named locally reacting liners [2].

In absence of flow, acoustic liners are modelled as mass-spring-damper systems and are therefore characterized by a resonant frequency [3]. The interaction of an acoustic wave with the resonator can be described through the concept of acoustic impedance $Z = \theta + i\chi$, which is defined in the frequency domain as the ratio between the Fourier components of the acoustic pressure and of the acoustic velocity normal to the liner. The impedance is a complex number, which associates dissipative and inertial fluid behaviour to the resistive θ and reactive χ components, respectively. The acoustic impedance can be used to model the effect of liners on the surrounding acoustic field through an ad hoc boundary condition for a wave propagation problem [4]. In realistic engine operating regimes, a turbulent grazing flow is present and the amplitude of the acoustic wave is large, thus resulting in a non-linear response of the liner. In these conditions, several fundamental issues connected with the theoretical modelling of impedance arise [5–7], and even the definition of impedance is questionable [1, 2].

Experiments showed that, in presence of a flow, the educed impedance depends on the direction of the sound wave relative to the mean flow direction [2, 8, 9]; this result goes against the definition of locally-reacting liner. This finding was attributed to the use of the Ingard-Myers boundary condition [10] in the impedance eduction techniques. As a matter of fact, this boundary condition neglects the viscous effects, which are essential for modelling the acoustic wave-turbulent boundary layer interaction [11, 12]. In a recent paper, Weng et al. [2] proposed two eduction techniques where they used the linearized Navier-Stokes equations and turbulence models to include both the viscous effects and the influence of the turbulent boundary layer. Despite this, they did not resolve the wave direction dependence concluding that other physical phenomena, not identified yet, should be considered to characterize the acoustic liners.

To clarify how the interaction between the acoustic waves and the turbulent boundary layer affect the noise dissipation mechanism, detailed information of the in-orifice fluid dynamics is necessary. More in detail, it is necessary to characterize how vorticity, generated by the shear forces at the orifice walls, is affected by the presence of the turbulent flow. The small dimensions of the acoustic liners makes the measurements of these phenomena very complex. For this reason, numerical simulations of the unsteady flow can be used [1, 13–18]. Tam et al. [17] complemented experimental measurements and two-dimensional Reynolds Average Navier-Stokes (RANS) simulations to study a multi-resonator liner mounted in a grazing flow duct. They found that, in presence of a grazing flow, acoustic liners produce self-noise generated via a feedback acoustic resonance mechanism. Zhang and Bodony [1] performed Direct Numerical Simulation (DNS) of a conventional single-degree-of-freedom locally-reacting acoustic liner tested in the NASA Langley Grazing Flow Impedance Tube (GFIT) [19]. They simplified the acoustic liner considering a single orifice instead of multiple orifices for each honeycomb structure, imposed a temporally evolving boundary layer and performed computations at low scaled Reynolds number. They found three velocity scales that describe the flow within the cavity. Starting from these quantities, they proposed a reduced-order model for the in-orifice flow and a time-domain impedance model. Since the computational effort to simulate the flow over a full liner is too large, Sebastian et al. [18] performed a

Large Eddy Simulation (LES) of a compressible channel flow with impedance boundary conditions to model the liner. They observed, for liners with low resonance frequency and resistance, the presence of surface waves above the liner. These waves, with wavelength larger than the turbulent flow structures, modulate the turbulent structures and transport momentum toward the surface causing drag increase. This phenomenon might have an effect on the in-orifice flow, but a computational or experimental proof in presence of cavities is missing.

As seen from the brief literature review, understanding of the in-orifice flow dynamic over a full acoustic liner is far from being achieved. Furthermore, the effect of a spatially-developing turbulent boundary layer and multi-orifice hydrodynamic interaction has not been addressed yet. Given the large computational effort needed for a DNS simulation of a full acoustic liner with multiple orifices for each honeycomb structure, but still with the aim of reproducing a realistic scenario, we have performed a lattice–Boltzmann Very Large Eddy Simulations (LB–VLES) of a realistic single-degree-of-freedom locally-reacting liner, where the cavity flow is simulated. The computations are carried out using the solver 3DS-Simulia PowerFLOW 5.4b.

The paper is structured as follows. First the computational approach and the methodology used to compute the impedance are presented in section II. Then, numerical results are compared with the experimental measurements in section IV. The analysis of the results, particularly focusing on the vorticity generation within the orifice and the multi-orifice interaction is discussed in section V. The main findings are summarized in the conclusions.

II. Methodology

A. Flow solver

The LB method is used to compute the flow field because it was shown to be accurate and efficient in presence of complex flow problems and simulations of acoustic liners in a normal impedance tube configuration [20–24]. The commercial software 3DS Simulia PowerFLOW 5.4b is used. The software solves the discrete LB equation for a finite number of directions. For a detailed description of the method, the reader can refer to Succi [25] and Shan et al. [26], while to Chen and Doolen [27] for a review. The LB method determines the macroscopic flow variables starting from the mesoscopic kinetic equation, i.e. the LB equation. The discretization used for this particular application consists of 19 discrete velocities in three dimensions (D3Q19), involving a third-order truncation of the Chapman-Enskog expansion [28]. The distribution of particles is solved by means of the LB equation on a Cartesian mesh, known as a lattice. An explicit time integration and a collision model are used. For the collision term, the formulation based on a unique Galilean invariant [29] is used. The equilibrium distribution of Maxwell-Boltzmann is adopted [28].

A Very Large Eddy Simulation (VLES) model is implemented to take into account the effect of the sub-grid unresolved scales of turbulence. Following Yakhot and Orszag [30], a two-equations $k - \epsilon$ Renormalization Group (RNG) is used to compute a turbulent relaxation time that is added to the viscous relaxation time. To reduce the computational cost, a pressure-gradient-extended wall-model (PGE-WM) is used to approximate the no-slip boundary condition on solid walls [31, 32]. The model is based on the extension of the generalized law-of-the-wall model [33] to take into account the effect of pressure gradient. These equations are iteratively solved from the first cell close to the wall in order to specify the boundary conditions of the turbulence model. For this purpose, a slip algorithm [27], obtained as generalization of a bounce-back and specular reflection process, is used.

B. Impedance eduction

The two-microphone approach developed by Dean [34] is used to compute the impedance. This method estimates impedance by using acoustic pressure signals at two different microphone locations: at the face sheet (p_s) and at the back plate (p_b). The Dean's method assumes that the liner is locally reacting and the sound wave entering the cavity is completely reflected back, i.e. resulting in a standing wave inside the cavity. For an incident sound wave, $p_{inc} = p_\infty e^{i(\omega t - k_a y)}$, the reflected wave is $p_r = p_\infty e^{i(\omega t + k_a y)}$, where $\omega = 2\pi f$, k_a is the acoustic wave number and y is the wall normal direction. The resultant standing wave inside the cavity is given by:

$$p = p_{inc} + p_r = 2p_\infty e^{i\omega t} \cos(k_a y). \quad (1)$$

The linearised momentum equation in the wall normal direction can be written as:

$$\frac{\partial v_a}{\partial t} = -\frac{1}{\rho_\infty} \frac{\partial p}{\partial y}. \quad (2)$$

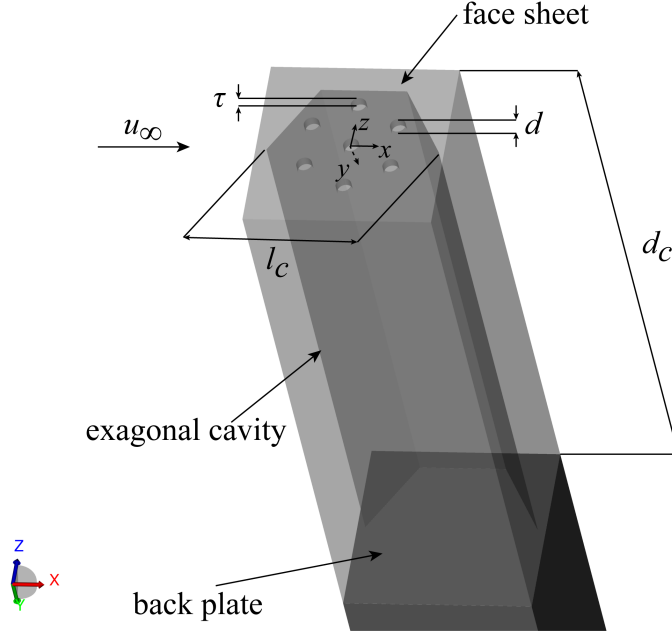


Fig. 1 Schematic of the cavity with representation of the coordinate reference system. The y axis is oriented towards the inside of the cavity.

Differentiating, equation 1 and integrating equation 2, the acoustic particle velocity v_a is:

$$v_a = -i \frac{2p_\infty}{\rho_\infty c_\infty} e^{i\omega t} \sin(k_a h), \quad (3)$$

where $\rho_\infty c_\infty$ is the characteristic impedance of the medium. Assuming that the acoustic particle velocity normal to the surface of the liner is identical to that inside the cavity, equation 3 can be rewritten as:

$$v_a = i \frac{2p_s}{\rho_\infty c_\infty} e^{i\omega t} \sin(k_a h). \quad (4)$$

From equation 1, we have that $p_b = 2p_\infty$. Then,

$$Z = \frac{p_s}{v_a} = i \frac{p_s}{p_b} e^{i\phi} \operatorname{cosec}(k_a h), \quad (5)$$

where ϕ is the phase difference between the pressure signals p_s and p_b .

III. Computational setup

The acoustic liner geometry investigated in the present study was also experimentally investigated by Jones et al. [19] in the GFIT facility at NASA Langley Research Center and computationally investigated by Zhang and Bodony [1]. It is sketched in figure 1. A rigid face sheet of thickness $\tau = 0.64$ mm is perforated with cylindrical holes of diameter $d = 0.99$ mm, which corresponds to a length-to-diameter ratio of 0.65. A single honeycomb cavity with 7 orifices is studied, thus resulting in a porosity of $\sigma = 6.4\%$ very close to the reference study. While in the experimental study the orifices are randomly located such that they can overlap neighboring cavities, in this study, six orifices are placed at the center of each of the six equilateral triangles that form the hexagon and one at its center. A sketch of the cavity is reported in figure 1. The face sheet is fixed to a honeycomb structure with a regular exagonal cell. The cell depth is $d_c = 38.10$ mm and the distance between the two opposite corners of the cell is $l_c = 9.5$ mm. A rigid back plate closes the cell from below and the cell walls are rigid, so that, in the experiments, neighboring cells cannot communicate.

The acoustic liner is grazed by a turbulent flow with free stream Mach number equal to $M_\infty = 0.3$ and an acoustic wave at a frequency f equal to 1800 Hz and amplitude equal to 130 dB, where the Sound Pressure Level (SPL) is computed using a reference pressure of 20×10^{-6} Pa. The liner is placed along the top wall of a duct that has a

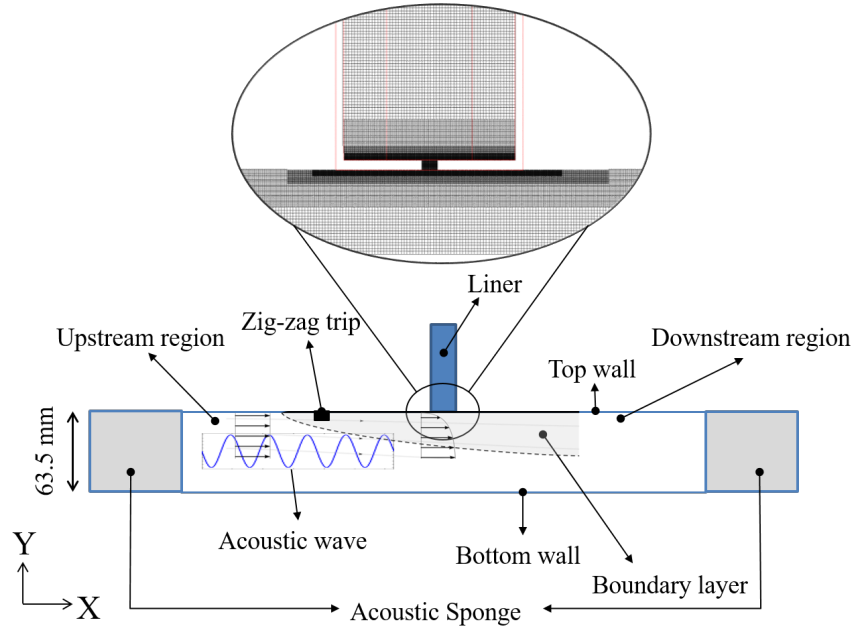


Fig. 2 Schematic of the computational setup with the grid in a plane crossing the central orifice.

rectangular cross section with height equal to 63.5 mm, as in the GFIT facility, while the width is restricted to 12 mm to reduce the computational cost. The length of the duct is equal to 4900 mm. This has been chosen such to fit 20 wavelengths of the acoustic wave to guarantee convergence of the results [23]. Transition to turbulence is forced using a zig-zag strip at 1750 mm upstream of the liner. The zig-zag strip is 1 mm thick, it has length and wavelength equal to 10 mm and angle of 60° . The location of the zig-zag strip has been selected such to replicate the time-average turbulent boundary layer profile of the experiments [35]. A schematic of the computational setup is reported in figure 2, where an example of the computational grid close to cavity is shown. In the computations, 10 resolution regions are used; the smallest voxels are used to discretize the computational domain close and within the orifices. The maximum resolution adopted in this paper is 30 voxels/mm ≈ 30 voxels/ d . This is slightly smaller than the value suggested by Manjunath et al. [23] in absence of acoustic waves of ≈ 42 voxels/ d . However, minor differences are expected in the estimation of Z . This is due to reduce the larger computational cost of this simulation with respect to case without grazing turbulent flow.

Periodic boundary conditions are applied on the side walls, no-slip boundary condition on the top wall and slip boundary condition on the bottom wall. At the inlet, free stream velocity corresponding to the free stream Mach number is assigned while pressure boundary condition is set at the outlet. Additional acoustic sponge regions, where viscosity is increased, are placed at the inlet and outlet of the computational domain to dampen the reflection of acoustic waves.

Computations are carried out with a two-step approach: first the turbulent boundary layer convecting in the duct is computed and convergence is verified; on the converged turbulent flow, an acoustic wave, with given frequency and amplitude, is superimposed and propagated in the duct.

Data is sampled at a frequency of 7975 Hz. For the estimation of the impedance, data is sampled only after a statistical steady state is reached.

IV. Validation

Validation of the computational methodology is performed through grid convergence study and comparison against experimental data [19, 35]. Validation is carried out to verify that both the integral turbulent boundary layer parameters and both components of the acoustic impedance Z match with the experiments. Three grid resolutions are investigated corresponding to 6, 15 and 30 voxels/ d . They are named respectively coarse, medium and fine resolution in the rest of the study.

First it is verified that the turbulent boundary agrees with the experimental one. For this purpose, simulations without the grazing acoustic wave are performed to locate the zig-zag trip such to match the turbulent boundary layer

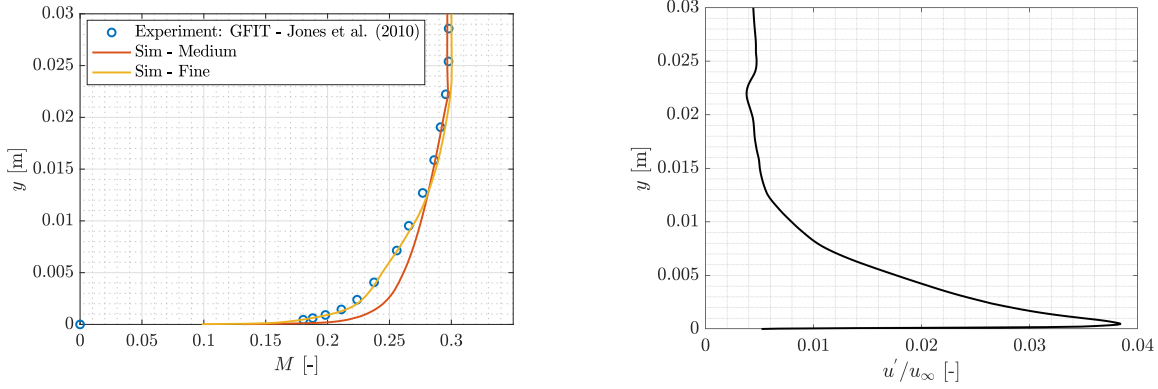


Fig. 3 (left) Time-averaged streamwise velocity profile and (right) profile of the turbulent fluctuation of the streamwise velocity component upstream of the liner. The time-average profile is also compared with the experimental results of Jones et al. [35].

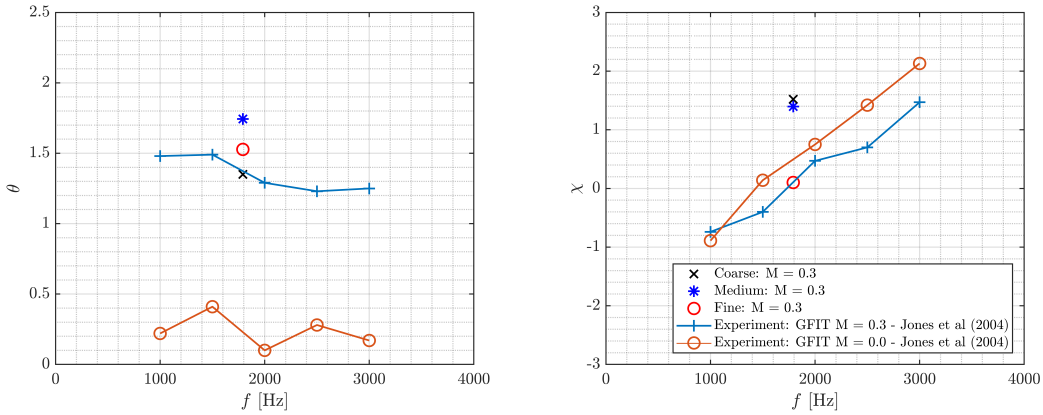


Fig. 4 Resistance θ and reactance χ components of the impedance Z for different grid resolutions and comparison with the experiments of Jones et al. [19].

profile. This was done with a trial and error approach. The location for the first attempt was obtained from the equation $\delta = 0.37x_t/Re_{x_t}^{1/5}$ [36], where δ is the boundary layer thickness, x_t is the distance downstream of the start of the turbulent boundary layer and Re_{x_t} is the Reynolds number evaluated at the location downstream of the trip.

The time-averaged boundary layer profile upstream of the liner is plotted in figure 3 (left). In this figure, the computational results are shown only for two resolutions (medium and fine) for the sake of clarity and compared with the experimental results [35]. The figure shows that, for the medium resolution, the flow close to the wall is not well resolved thus resulting in a flatter boundary layer with respect to the fine resolution configuration. For the higher resolution case, the boundary layer profile matches well with the experimental data. Since the interaction between a turbulent flow and a orifice is strongly dependent on the integral turbulent boundary layer parameters, in particular on the ratio δ^*/d [1], this suggests that the numerical solution can reproduce the interaction between the orifice and the turbulent flow.

The wall-normal distribution standard deviation of the streamwise velocity component fluctuations u' in the boundary layer for the fine case is plotted in figure 3 (right). The intensity of the turbulent fluctuations is about 4% of the free stream velocity. The amplitude of the velocity fluctuations is smaller than the expected one for a fully turbulent boundary layer. This suggests that an additional increase of resolution is necessary to well-capture the intensity of the turbulent fluctuations.

As discussed in the previous section, after it is verified that the turbulent boundary layer is similar to the experimental one, an acoustic wave is superimposed and pressure data around the orifices and on the back plate are sampled following Manjunath et al. [23]: pressure fluctuations on the surface of the liners p_s for each of the orifice is acquired at 12 points

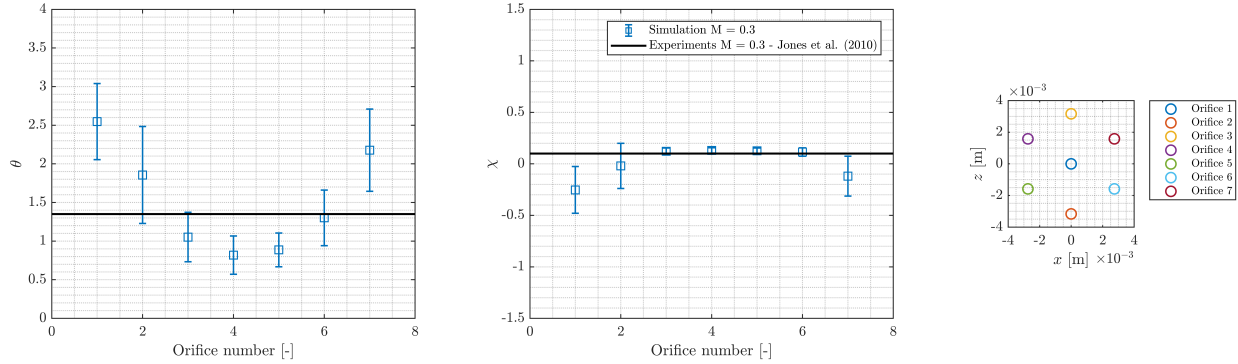


Fig. 5 Resistance θ and reactance χ components of the impedance Z for each of the 7 orifices. The spatial distribution of the orifices is plotted in the right subfigure.

surrounding each orifice, while pressure fluctuations at the back plate p_b are acquired at points aligned with the center of each orifice. Subsequently, the values obtained for the two components of the impedance are averaged. Results for the three grid resolutions are plotted in figure 4. In figure 4, the two components of the acoustic impedance Z the resistance θ and the reactance χ are plotted in the left and right subfigure respectively. In the same figure, the experimental results for both the grazing flow ($M = 0.3$) and the no-grazing flow ($M = 0.0$) configurations are reported. It is important to mention that the experimental results are obtained using an inverse approach and not with the Dean's method.

The comparison shows that the numerical results agree with the experimental one. The resistance shows a fluctuating behavior around the experimental value while the reactance shows an overestimation at low resolution in agreement with the previous study [23]. When comparing with the case without grazing flow ($M = 0.0$), the resistance θ shows larger variations with respect to the reactance χ . This can be attributed to the fact that the resistance is related to the dissipative behavior that is enhanced by the presence of the turbulent structures while the flow weakly affect the inertial behavior.

Even if an additional simulation with higher resolution would be necessary to full verify that the results are grid independent, the similarity of both the time-averaged turbulent boundary layer and of the acoustic impedance gives confidence that data can be used to analyze the interaction between multiple orifices and how a spatially developing turbulent boundary layer affects the liner behavior.

V. Results

In the previous section, the impedance Z calculated by averaging the local impedance obtained for each of the 7 orifices was shown. The spatially developing boundary layer and the turbulent wake behind each orifice can affect the local impedance. For this reason, the two components of the impedance computed for each orifice are plotted in figure 5. The location of each orifice is plotted in the subplot on the right hand side. The errorbar in the figures represents the scattering in the estimation of the impedance using the 12 time series from the equally spaced points on the face sheet around each orifice [23].

Results show that the resistance θ , plotted in the subfigure on the right hand side, varies spatially more than the reactance χ . The calculated impedance varies of about 3 times between the most upstream orifices and the most downstream ones. The former shows lower resistance and larger reactance with respect to the latter. This might be caused by two phenomena: at the face sheet, a turbulent wake, generated behind each orifice, can increase the velocity and pressure fluctuations; large scale vortex motions, generated by the interaction of the grazing flow with each orifice, can interact and affect the ejection of the vorticity generated within the orifice, thus affecting the pressure signal at the back plate. While for the former it is possible to verify the interaction between the turbulent wakes, for the latter it is not straightforward to separate the contribution of the flow through each orifice. As a general result, it is possible to state that, using a technique such as the Dean's method, the results might be strongly affected by the measurement location.

The effect of the grazing flow on a multi-orifice acoustic liner is further investigated by analyzing the cavity and near orifice flow features. First a snapshot of the instantaneous flow field in the $x - y$ plane at $z/d = 0$ (i.e., a plane aligned with the liner centerline) is plotted in figure 6 where streamlines are superimposed to contour of static pressure.

The figure shows plane acoustic waves grazing the liner; the amplitude of the acoustic wave decreases after convecting over the acoustic liner. The streamlines show that, because of the turbulent grazing flow, the flow through the orifice is

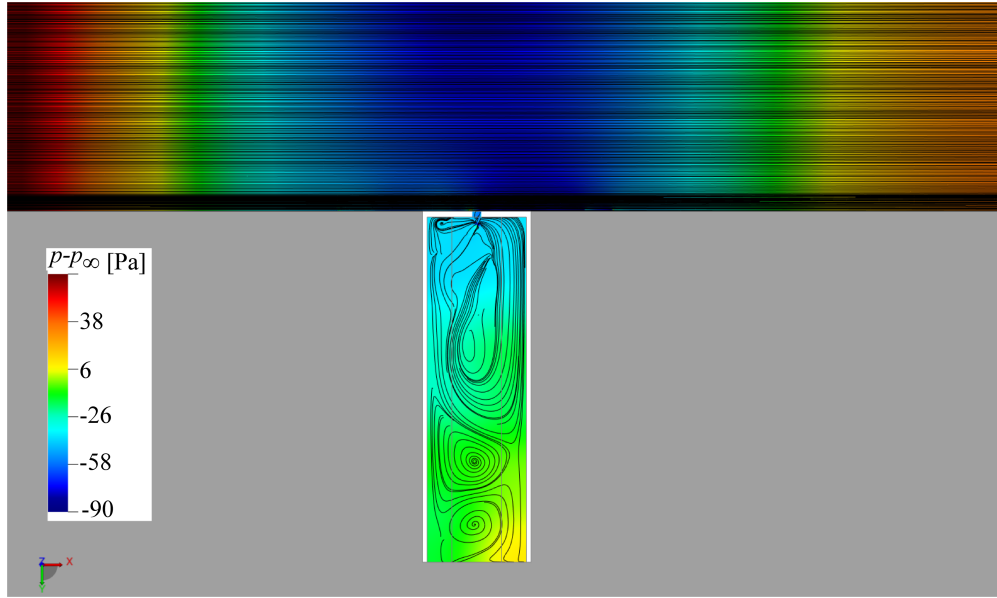


Fig. 6 Instantaneous flow visualization of the flow over the liner with superimposed acoustic wave. Contour of static pressure with superimposed streamlines.

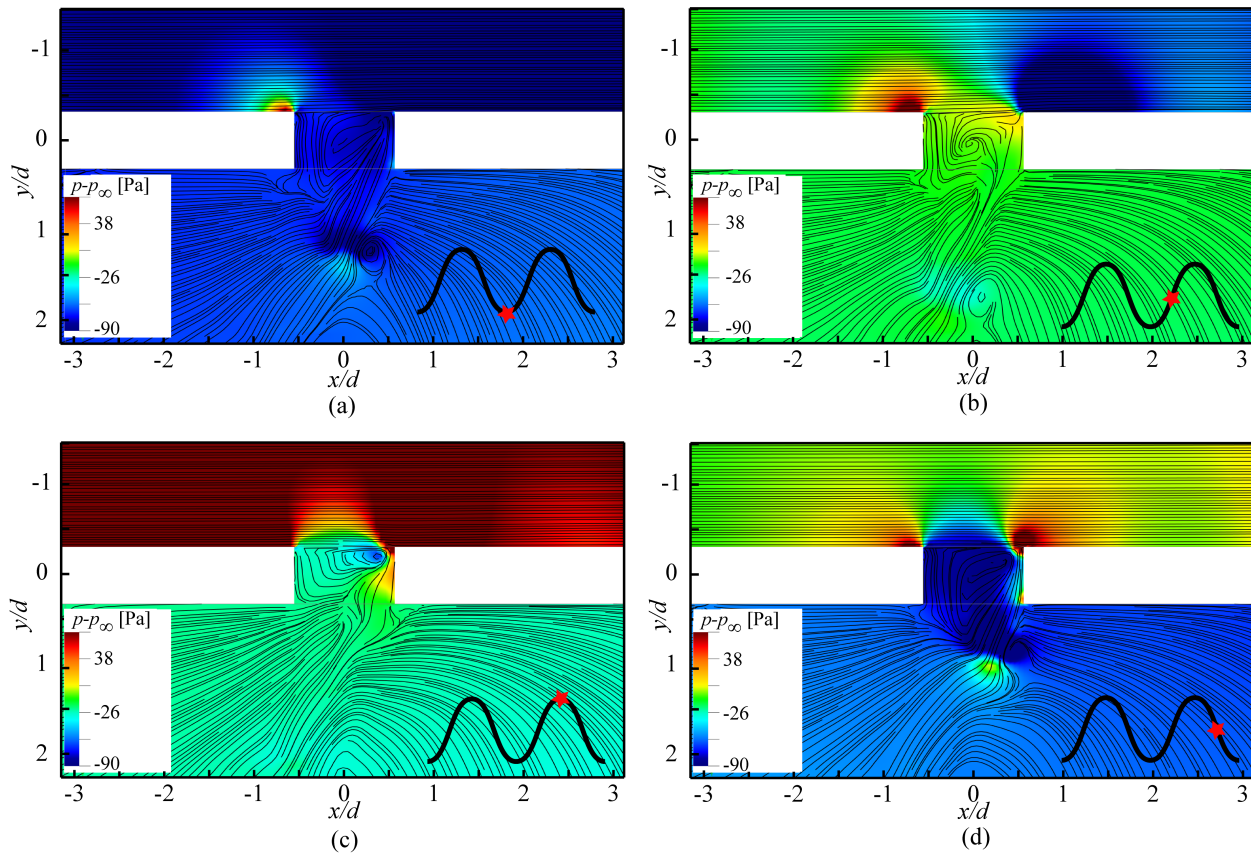


Fig. 7 Contour of static pressure with superimposed streamlines. Four phases, characteristic of the passage of the acoustic wave, are identified through the sketch on the bottom right side of each subfigure.

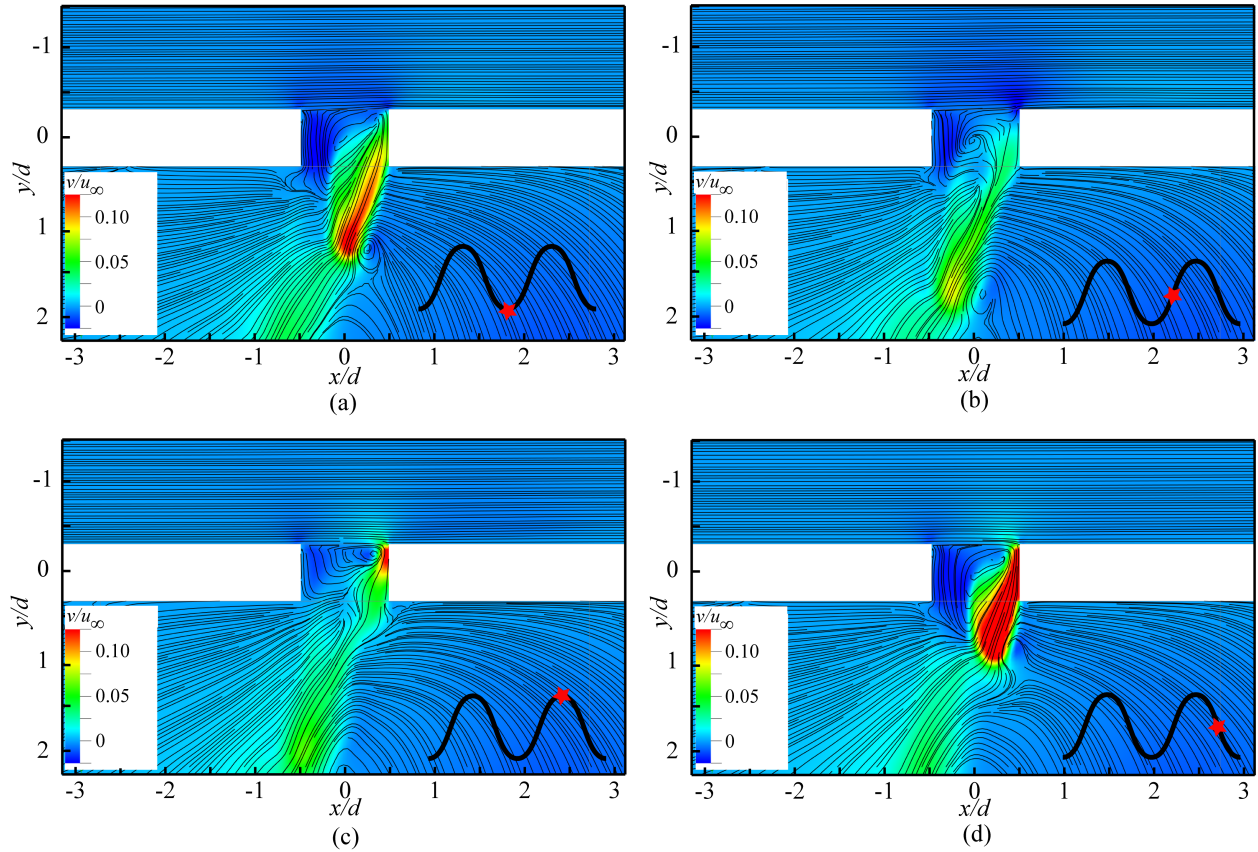


Fig. 8 Contour of the wall-normal velocity component with superimposed streamlines. Four phases, characteristic of the passage of the acoustic wave, are identified through the sketch on the bottom right side of each subfigure.

asymmetric, differently from the case with no grazing flow [1, 23], and the formation of multiple large scale vortical structures within the cavity. At this time instant, corresponding to the ejection phase of the vortices from the orifices, a small clock-wise rotating vortex is generated on the up-right corner, while three large scale vortices are visible at the bottom of the cavity. The clock-wise rotating vortex was also found in previous studies [1].

The analysis of the in-orifice flow, induced by both the grazing flow and acoustic wave, starts with a detailed description of the vortex generation and ejection. Figures 7 and 8 show close up of the instantaneous flow organization for the central orifice, with center at $z/d = 0$, at four phases, each of them is sketched on the bottom right hand side of each subfigure. Figure 7 shows contour of static pressure with superimposed streamlines, while figure 8 shows contour of the wall-normal velocity component, which is positive in the direction entering the cavity (figure 1).

Results show that vorticity is produced when the acoustic wave causes a local increase of pressure over the orifice (figure 7(c) and figure 8 (c)). Because of the grazing turbulent flow, the clockwise rotating vortex is pushed toward top right hand side of the orifice. The vortex grows in size while the acoustic wave, which has wavelength larger than the orifice diameter, passes over the orifice. Then, fluids is entrained from the right hand side of the orifice transferring momentum into the cavity. Because of the presence of the central vortex, fluid on the right hand side of the cavity is accelerated and the shear at the wall increases. The flow entering the cavity from the right hand side rolls up around the corner on the bottom hand right side generating an anticlockwise rotating vortex (figure 7(d) and figure 8 (d)), that is then ejected into the cavity convecting in the negative x direction. This vortex dissipates while convecting into the cavity, while the vortex formed at the center of the cavity dissipates vorticity at the center of the cavity. Because of the asymmetry of the vortex generation, the annular vortices ejected into the cavity are subject to strong azimuthal deformation, which allows them to be coherent for a longer distance with respect to conventional vortices thus increasing the peak velocity with respect to the conventional annular jet [37]. The maximum wall normal velocity component into the orifice at the phase sheet location is about $0.015u_{\infty}$, that is in agreement with what was found by Zhang and

Bodony [1] for a similar amplitude of the grazing acoustic wave. The vortex generated on the vertex on the bottom right hand side penetrates into the cavity up to 3 orifice diameters, while the one formed at the center of the orifice does not exit it in agreement with previous literature [1]. As visible from figure 7(d) and figure 8 (d), the wake of the ejected vortex, generated during the previous cycle, is still visible and might be pushed within the cavity, thus increasing the penetration depth of the vorticity. It is worth to mention that, in the DNS results of Zhang and Bodony [1], this secondary vortex was not detected and that its convection within the cavity might affect the measurement of impedance using the low order model they proposed. The vortex locked into the orifice pushes fluids in the negative y direction on the left hand side of the orifice, thus being an obstacle for the flow penetration within the orifice at this location. This causes a local increase of pressure (visible in figure 7(a) and figure 8 (a)), which might cause flow separation just upstream of the cavity that generates vorticity that convects on the face sheet as will be discussed below.

To investigate how the flow structures, generated within each orifice, are ejected into the cavity, iso-surface of λ_2 criterion for vortex identification color-contoured with static pressure are plotted in figures 9. The same four phases as for the previous analysis are shown. Information on the phase can be retrieved by the wall-normal slice where the static pressure distribution indicates the phase of the grazing plane acoustic wave. This is further reported in the sketch on the bottom of each subfigure. Streamlines, used to detect large scale vortex motions, are super-imposed to the wall-normal slice. In figure 9, the wall normal slice in the $x - y$ plane is at $z/d = 0$, i.e. a plane aligned with the central orifice center line.

Iso-surfaces show that, at the face sheet, for orifices with center at the same z/d location, the wake behind the upstream orifice interacts with the downstream orifice. Within the cavity, there is no visible large scale interaction between the vortices ejected from the orifice. The ejected vortices are characterized by an annular vortex, induced by the shear of the flow pushed within the cavity (figure 7(a) and figure 8 (a)), and trailing vortices (figure 9 (a)). These features of the ejected vortices are the ones found in synthetic jets [37]; a trailing vortex is present in the wake of a annular jet. For the current setup, focusing on the vortical structures generated by the two orifices with centers at the same z/d location, it can be noticed that, during the ejection phase, two annular vortices are still present in the near wake of the jet ejected by the downstream orifice while only one is present for the upstream orifice. On the same line, for the upstream orifice, the ejected vortex is still connected to the orifice when a new vortex is generated while for the downstream one it is already disconnected. This can be due to the effect of the upstream wake on the flow within the orifice. In addition, the former shows a different ejection direction with respect to the upstream one; more downstream vortices are less aligned in the y direction.

This is better visualized in figure 10 where, for a given phase, two additional wall-normal planes crossing the centers of the orifices are plotted, i.e. $z/d = 1.65$ and $z/d = 3.25$. These figures show that the vortices ejected by the orifices, located closer to the upstream walls of the cavity, are more aligned in the y direction. The vicinity to the walls affects also the location and the formation of the large scale structures in the cavity. Comparing the different wall-normal slices, it is evident that the anticlockwise rotating vortex formed close to the face sheet becomes weaker and disappears in the other two planes. Similarly, the core of the large clockwise rotating vortex is located at different y locations, i.e. closer to the face sheet further from the center of the cavity. These findings suggest that the flow within the cavity is strongly three-dimensional and can affect the generation and ejection of the vortices generated through the orifices. This might affect the discharge coefficient, thus having an effect on the deduced impedance.

As mentioned at the beginning of the discussion, for a multi-orifice liner, at the face sheet, the wake behind an upstream orifice can interact with a downstream orifice thus affecting local measurement of impedance. To study this interaction, the streamwise u and wall-normal velocity v components at the first cell near the wall are plotted in figures 11 and 12, respectively. The selected phases are the same as the previous figures.

Results show that for this configurations, only orifices with centers at the same spanwise location of the upstream ones are affected by the wake. However, the lateral spreading of the wakes is such that, if another cavity would be present, with a similar distribution of orifices, they would be all affected by the upstream turbulent induced flow. Results show that this interaction has an effect on the in-orifice flow. As a matter of fact, the recirculation region behind the orifice is smaller than the separation length between orifices. Then a transitional wake is formed with additional near-wall flow structures of size comparable with the orifice diameter, thus being able to affect the near orifice flow. Because of this interaction, the downstream orifices show a more uniform spanwise distribution of velocity in the streamwise direction and a shorter recirculation length in the near wake. More in detail, during the generation phase of the vortices (figure 11 (c) and figure 12(c)), the upstream orifices show peaks along the centerline direction for both the streamwise and wall-normal velocity components while the downstream orifices show a more uniform spatial distribution. The maximum wall-normal velocity component is about $0.03u_\infty$, which is comparable with results from previous literature [1]. Additionally, the downstream orifices show a longer part of the orifice diameter, in the streamwise direction, with

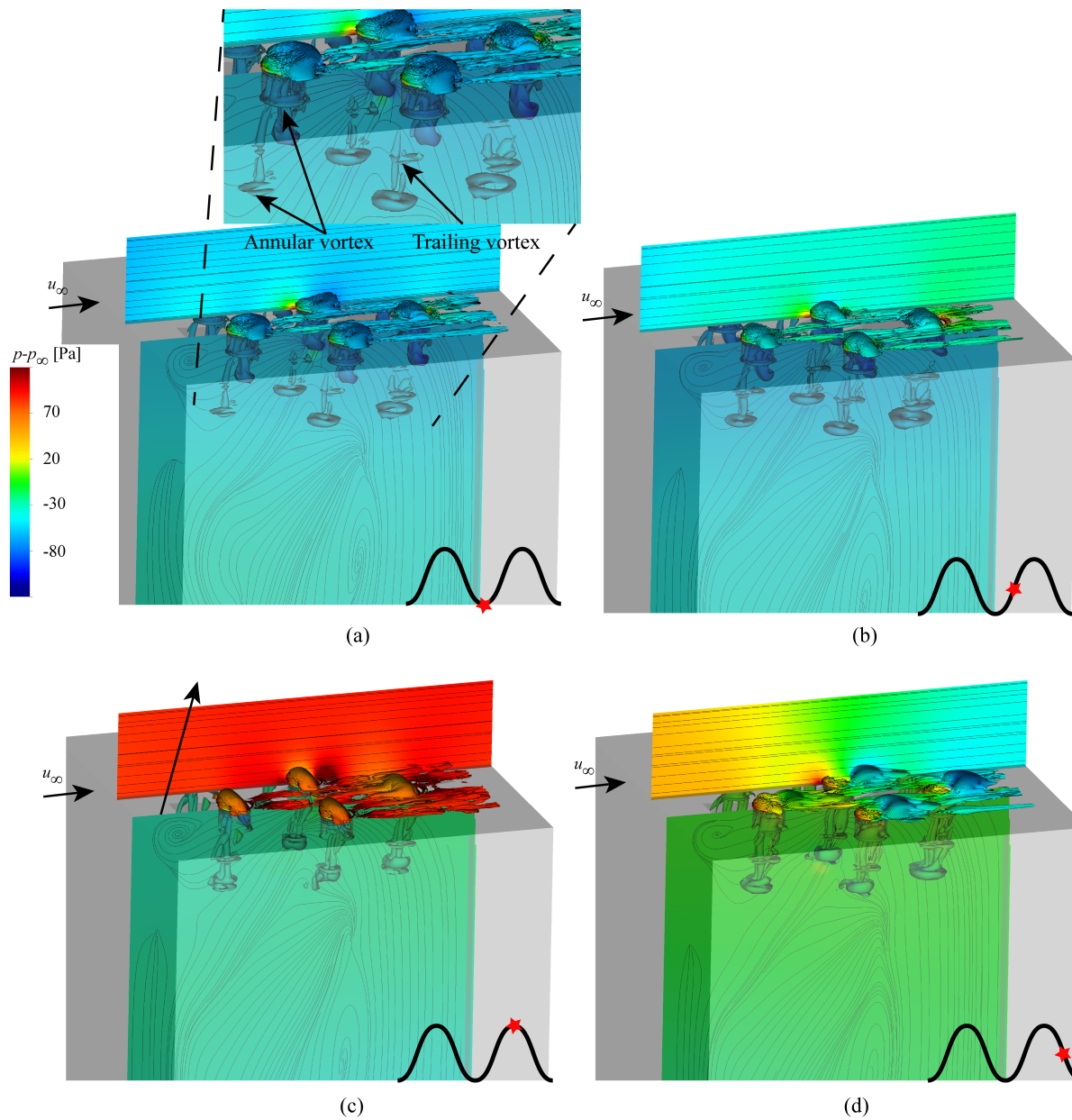


Fig. 9 Iso-surface of the λ_2 criterion for vortex visualization. Contour of the static pressure super imposed with streamlines on the wall-normal slice at $z/d = 0$. Four phases, characteristic of the passage of the acoustic wave, are identified through the sketch on the bottom right side of each subfigure.

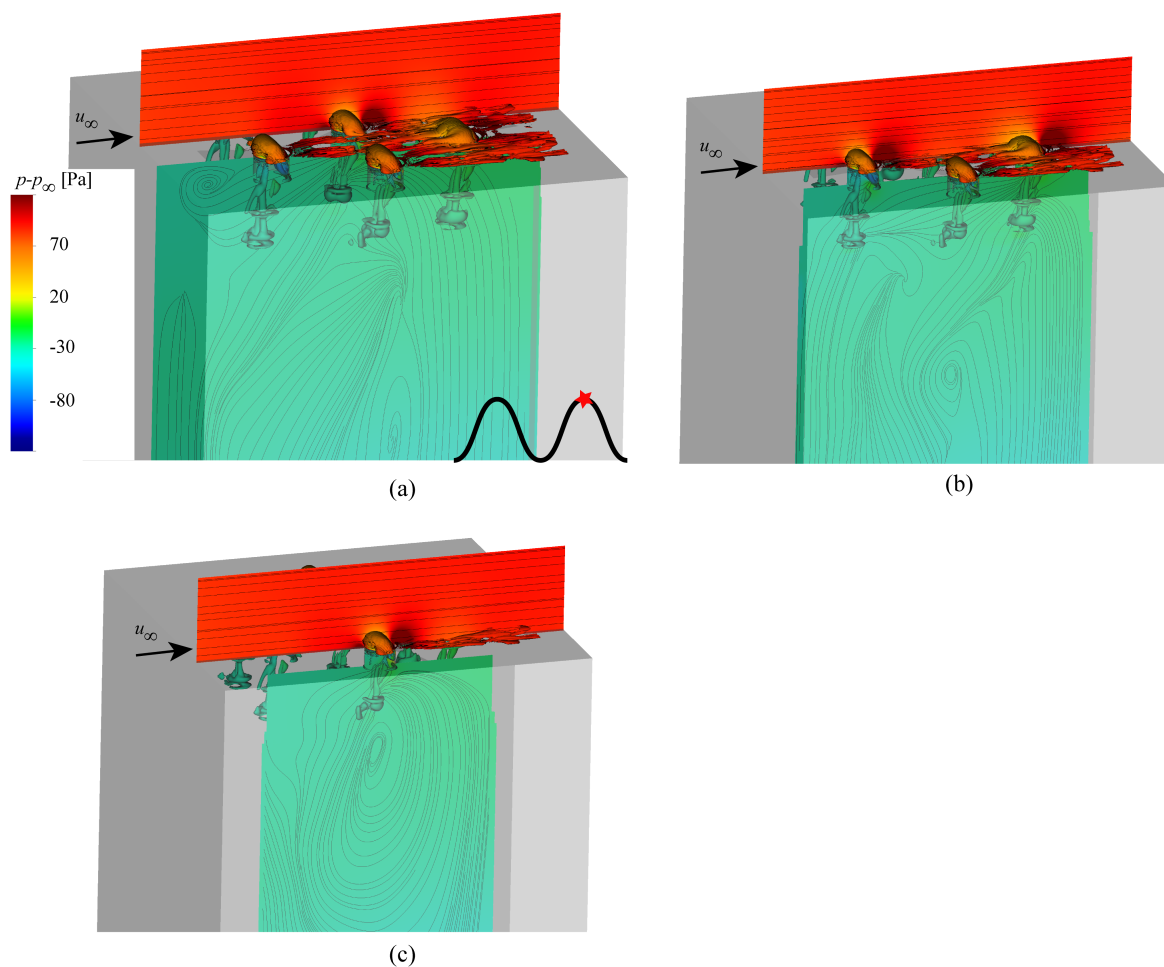


Fig. 10 Iso-surface of the λ_2 criterion for vortex visualization. Contour of the static pressure super imposed with streamlines on the wall-normal slice at $z/d = 0$ (a), $z/d = 1.65$ (b), $z/d = 3.25$ (c). The phase, characteristic of the passage of the acoustic wave, is identified through the sketch on the bottom right side of each subfigure.

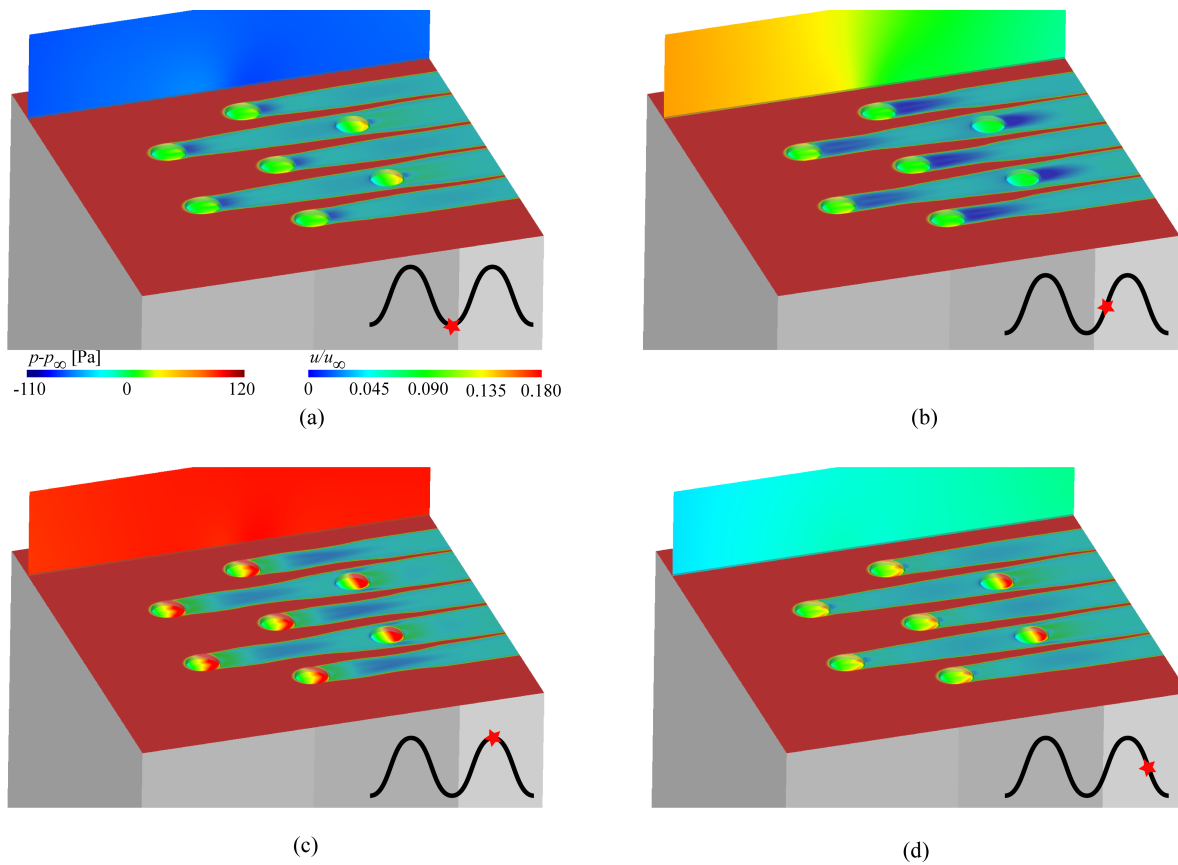


Fig. 11 Contour of the streamwise velocity component u on the wall-parallel plane and contour of the static pressure on the wall-normal plane. The phase, characteristic of the passage of the acoustic wave, is identified through the sketch on the bottom right side of each subfigure.

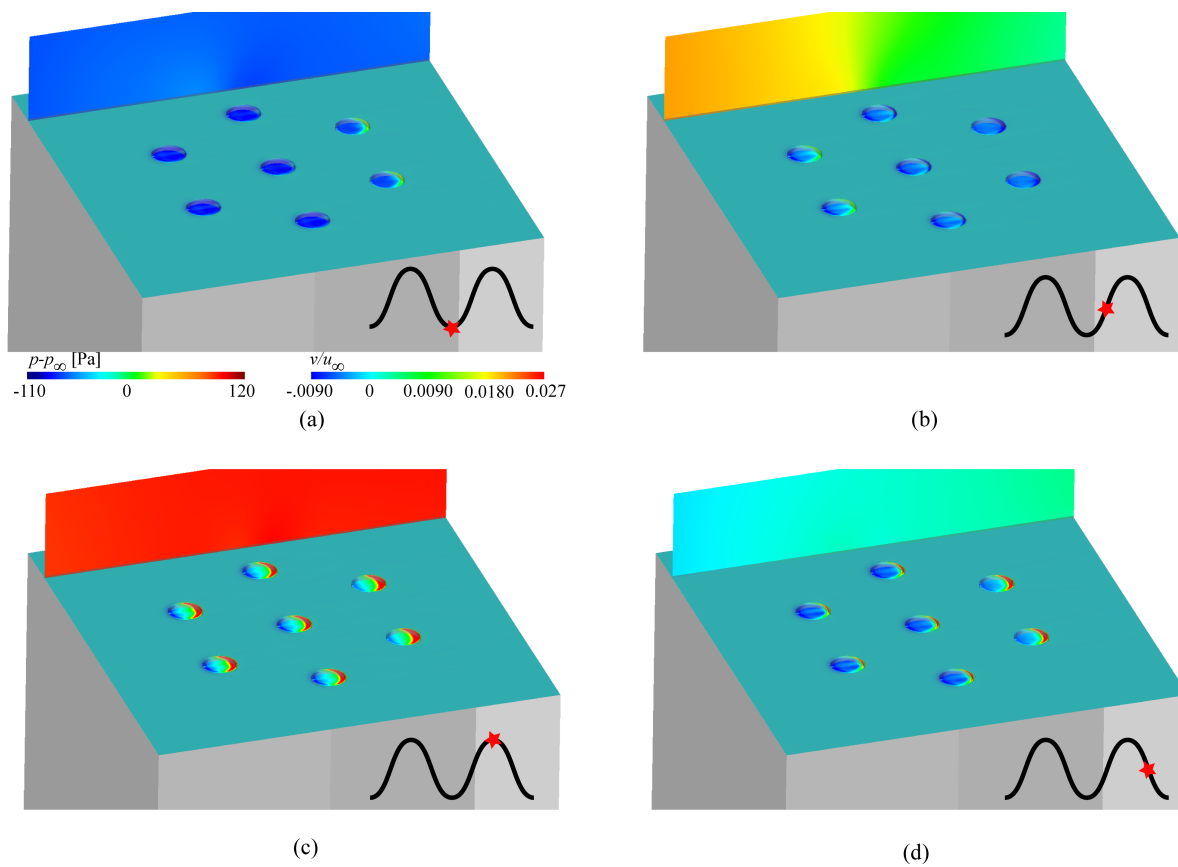


Fig. 12 Contour of the wall-normale velocity v on the wall-parallel plane and contour of the static pressure on the wall-normal plane. The phase, characteristic of the passage of the acoustic wave, is identified trough the sketch on the bottom right side of each subfigure.

higher ν with respect to the upstream orifices. This might suggest the differences in the size of the vortical structures within the cavity observed in figure 9. This confirms that the integral boundary layer parameters can play an important role in the interaction, particularly when near wall coherent flow structures are present.

VI. Conclusions

A lattice-Boltzmann Very Large Eddy Simulation of a multi-orifice acoustic liner grazed by a turbulent flow at Mach number equal to 0.3 and a planar acoustic wave with amplitude equal to 130 dB and frequency equal to 1800 Hz is carried out. The simulations replicates the experiments carried out in the GFIT facility at NASA Langley, which data are used for comparison. A two-step simulation approach is used: first the turbulent flow over the acoustic liner is obtained and verified through a convergence study; then the acoustic wave, with given SPL and frequency, is superimposed to the turbulent flow and convected in the cavity. This allows for reduction of the computational cost when multiple acoustic waves needs to be tested, because the computational cost associated with the second simulation is one order of magnitude smaller than the one of the first step.

The time-averaged turbulent boundary layer is compared with the experimental reference data [35] showing good agreement. Similarly, both components of the acoustic impedance, i.e. the resistance and the reactance, obtained by averaging the local impedance of each orifice measured with the Dean's method, are similar to the experimental ones [19]. Comparing the impedance measured for each orifice, it is found that it varies with the orifice location and that the local value depends on the location of the probes used for its estimation. From a preliminary analysis of the flow features within the cavity and at the face sheet, it is found that this can be attributed to two phenomena: the interaction between the wakes downstream of the upstream orifices with the downstream ones; and the interaction between the vortices ejected in the cavity and the cavity walls. It is found that, for this particular configuration, two vortices are generated in the orifice: one, generated at the downstream side of the orifice, weakly penetrates into the cavity; the second is generated at the bottom downstream corner of the orifice and is ejected into the cavity up to 3 orifice diameters. The direction of ejection of the latter depends on the spatial location of the orifice. These vortices are characterized by an annular vortex and a trailing vortex similarly to what found for synthetic jets. The cavity is further characterized by large scale vortical structures that are bend. On the face sheet, the flow within the orifice is affected by the turbulent wakes behind the upstream orifices that generates additional near-wall turbulent flow structures with size smaller or comparable with the orifice diameter, thus yielding a more spanwise uniformity of the flow into the orifice and longer streamwise length of the orifice diameter with larger wall-normal velocity component.

The current dataset will be further verified with a higher resolution simulation and it will be used to verify and improve low order fidelity models for the prediction of acoustic impedance with a particular focus on non-linear effects.

Acknowledgment

The authors would like to thank Dr. M. Jones (NASA Langley Research Center) for sharing the experimental data. Simulations were carried out on the Cartesius HPC under the NWO grant number 16918-5579.

References

- [1] Zhang, Q. and Bodony, D., "Numerical investigation of a honeycomb liner grazed by laminar and turbulent boundary layers," *Journal of Fluid Mechanics*, Vol. 792, apr 2016, pp. 936–980.
- [2] Weng, C., Schulz, A., Ronneberger, D., Enghardt, L., and Bake, F., "Flow and Viscous Effects on Impedance Education," *AIAA Journal*, dec 2017, pp. 1–15.
- [3] Olivetti, S., Sandberg, R., and Tester, B., "Direct numerical simulation of turbulent flow with an impedance condition," *Journal Sound and Vibration*, Vol. 344, 2015, pp. 28–37.
- [4] Brambley, E., "Review of acoustic liner models with flow," *Acoustics*, 2012, pp. 3429–3434.
- [5] Singh, D. and Rienstra, S., "Nonlinear asymptotic impedance model for a Helmholtz resonator liner," *Journal of Sound and Vibration*, Vol. 333, No. 15, jul 2014, pp. 3536–3549.
- [6] Khamis, D. and Brambley, E., "Acoustic boundary conditions at an impedance lining in inviscid shear flow," *Journal of Fluid Mechanics*, Vol. 796, jun 2016, pp. 386–416.

- [7] Rienstra, S. and Singh, D., “An asymptotic model for non-linear Helmholtz resonator of finite depth,” *22nd AIAA/CEAS Aeroacoustics Conference*, American Institute of Aeronautics and Astronautics, Reston, Virginia, may 2016.
- [8] Renou, Y. and Aurégan, Y., “Failure of the Ingard–Myers boundary condition for a lined duct: An experimental investigation,” *The Journal of the Acoustical Society of America*, Vol. 130, No. 1, jul 2011, pp. 52–60.
- [9] Boden, H., Cordioli, J., Spillere, A., and Serrano, P., “Comparison of the effect of flow direction on liner impedance using different measurement methods,” *23rd AIAA/CEAS Aeroacoustics Conference*, American Institute of Aeronautics and Astronautics, Reston, Virginia, jun 2017.
- [10] Myers, M. K., “On the acoustic boundary condition in the presence of flow,” *Journal of Sound and Vibration*, Vol. 71, No. 3, aug 1980, pp. 429–434.
- [11] Aurégan, Y., Starobinski, R., and Pagneux, V., “Influence of grazing flow and dissipation effects on the acoustic boundary conditions at a lined wall,” *The Journal of the Acoustical Society of America*, Vol. 109, No. 1, jan 2001, pp. 59–64.
- [12] Zhou, L. and Bodén, H., “A systematic uncertainty analysis for liner impedance reduction technology,” *Journal of Sound and Vibration*, Vol. 356, nov 2015, pp. 86–99.
- [13] Tam, C., Kurbatsii, K., Ahuja, K., and Gaeta, R., “A numerical and experimental investigation of the dissipation mechanisms of resonant acoustic liners,” *Journal of Sound and Vibration*, Vol. 245, No. 3, aug 2001, pp. 545–557.
- [14] Tam, C., Ju, H., Jones, M., Watson, W., and Parrott, T., “A computational and experimental study of resonators in three dimensions,” *Journal of Sound and Vibration*, Vol. 329, 2010, pp. 5164–5193.
- [15] Zhang, Q. and Bodony, D., “Numerical Simulation of Two-Dimensional Acoustic Liners with High-Speed Grazing Flow,” *AIAA Journal*, Vol. 49, No. 2, feb 2011, pp. 365–382.
- [16] Zhang, Q. and Bodony, D., “Numerical investigation and modelling of acoustically excited flow through a circular orifice backed by a hexagonal cavity,” *Journal of Fluid Mechanics*, Vol. 693, feb 2012, pp. 367–401.
- [17] Tam, C., Pastouchenko, N., Jones, M., and Watson, W., “Experimental validation of numerical simulations for an acoustic liner in grazing flow: Self-noise and added drag,” *Journal of Sound and Vibration*, Vol. 333, No. 13, jun 2014, pp. 2831–2854.
- [18] Sebastian, R., Marx, D., Fortuné, V., and Lamballais, E., “Numerical simulation of a compressible channel flow with an acoustic liner,” *23rd AIAA/CEAS Aeroacoustics Conference*, 2017, pp. AIAA 2017–4034.
- [19] Jones, M., Watson, W., Parrott, T., and Smith, C., “Design and Evaluation of Modifications to the NASA Langley Flow Impedance Tube,” *10th AIAA/CEAS Aeroacoustics Conference*, American Institute of Aeronautics and Astronautics, Reston, Virginia, may 2004.
- [20] Khorrami, M., Fares, E., and Casalino, D., “Towards Full Aircraft Airframe Noise Prediction: Lattice Boltzmann Simulations,” *20th AIAA/CEAS Aeroacoustics Conference*, American Institute of Aeronautics and Astronautics, Atlanta, Georgia, 2014, pp. AIAA 2014–2481.
- [21] Casalino, D., Hazir, A., and Mann, A., “Turbofan Broadband Noise Prediction Using the Lattice Boltzmann Method,” *AIAA Journal*, sep 2017, pp. 1–20.
- [22] Hazir, A. and Casalino, D., “Effect of Temperature Variations on the Acoustic Properties of Engine Liners,” *23rd AIAA/CEAS Aeroacoustics Conference*, American Institute of Aeronautics and Astronautics, Reston, Virginia, jun 2017.
- [23] Manjunath, P., Avallone, F., Casalino, D., Ragni, D., and Snellen, M., “Characterization of Liners using a Lattice-Boltzmann Solver,” *2018 AIAA/CEAS Aeroacoustics Conference*, American Institute of Aeronautics and Astronautics, Atlanta, Georgia, jun 2018.
- [24] Avallone, F., Van Der Velden, W., Ragni, D., and Casalino, D., “Noise reduction mechanisms of sawtooth and combed-sawtooth trailing-edge serrations,” *Journal of Fluid Mechanics*, Vol. 848, 2018.
- [25] Succi, S., *The lattice Boltzmann equation for fluid dynamics and beyond*, Clarendon Press, Oxford, 1st ed., 2001.
- [26] Shan, X., Yuan, X.-F., and Chen, H., “Kinetic theory representation of hydrodynamics: a way beyond the Navier–Stokes equation,” *Journal of Fluid Mechanics*, Vol. 550, 2006, pp. 413–441.
- [27] Chen, S. and Doolen, G., “Lattice Boltzmann method for fluid flows,” *Annual Review of Fluid Mechanics*, Vol. 30, No. 1, jan 1998, pp. 329–364.

- [28] Chen, H., Chen, S., and Matthaeus, W., “Recovery of the Navier-Stokes equations using a lattice-gas Boltzmann method,” *Physical Review A*, Vol. 45, No. 8, apr 1992, pp. R5339–R5342.
- [29] Chen, H., Zhang, R., and Gopalakrishnan, P., “Lattice Boltzmann Collision Operators Enforcing Isotropy and Galilean Invariance,” aug 2015.
- [30] Yakhot, V. and Orszag, S., “Renormalization group analysis of turbulence. I. Basic theory,” *Journal of Scientific Computing*, Vol. 1, No. 1, 1986, pp. 3–51.
- [31] Teixeira, C., “Incorporating Turbulence Models into the Lattice-Boltzmann Method,” *International Journal of Modern Physics C*, Vol. 09, No. 08, dec 1998, pp. 1159–1175.
- [32] Wilcox, D., *Turbulence modelling for CFD (Third Edition)*, DCW Industries, Incorporated, 2006.
- [33] Launder, B. and Spalding, D., “The numerical computation of turbulent flows,” *Computer Methods in Applied Mechanics and Engineering*, Vol. 3, No. 2, mar 1974, pp. 269–289.
- [34] Dean, P., “An in situ method of wall acoustic impedance measurement in flow ducts,” *Journal of Sound and Vibration*, Vol. 34, No. 1, may 1974, pp. 97–IN6.
- [35] Jones, M., Watson, W., and Nark, D., “Effects of Flow Profile on Educued Acoustic Liner Impedance,” *16th AIAA/CEAS Aeroacoustics Conference*, American Institute of Aeronautics and Astronautics, Reston, Virigina, jun 2010.
- [36] Schlichting, H. and Gersten, K., *Boundary-Layer Theory*, Springer-Verlag Berlin Heidelberg, 9th ed., 2017.
- [37] Crispo, C., Greco, C., Avallone, F., and Cardone, G., “On the flow organization of a chevron synthetic jet,” *Experimental Thermal and Fluid Science*, Vol. 82, 2017.